Journal of Engineering Physics and Thermophysics, Vol. 81, No. 6, 2008

ERRORS IN MEASURING THE TEMPERATURE OF METALS BY PYROMETERS BASED ON TRICOLOR MULTIELEMENT PHOTODETECTORS

A. G. Sen'kov and V. A. Firago

UDC 536/521

This paper considers a method for measuring the temperature of metals by pyrometers based on tricolor multielement photodetectors and analyzes its inherent errors.

Introduction. Temperature control of metal articles and blanks subjected to heat treatment at engineering plants is of great importance for providing high-quality products. For a number of reasons (high temperatures, movement of objects to be measured, strong electromagnetic fields in induction furnaces, etc.) it is customary to carry out this control by contactless methods. The pyrometric methods of temperature determination are based on the recording and analysis of the heat radiation characteristics of the object under investigation, i.e., on indirect measurements. Therefore, the main problem here is comparison of the thermodynamic temperature of the object to the recorded heat flow. In so doing, it is necessary to take into account the influence of the change in the object's emissivity ε with the wavelength λ and its temperature T, of the distance and angle of observation, the degree of the surface roughness and the kind of the material, the absorption of radiation by the medium between the pyrometer and the object being controled, the geometric parameters of the optical system, and the ambient temperature T on the measurement data. The methods of pyrometric control used in the industry do not permit measuring the thermodynamic (true) temperature of heated metals in the absence of information (or its lack) on the emissivity. The multispectral methods of monochromatic pyrometry [1–3] make it possible to considerably decrease the T measurement error caused by the indeterminacy of ε. However, in using them, one has to employ narrow-band optical filters, which complicates the design and increases the cost of the pyrometer, as well as decrease the signal-to-noise ratio of pyrometric signals at a low measured temperature. To increase the signal-to-noise ratio and exclude the influence of scale on the measurement data, one can use multielement photodetectors with several wide spectral ranges of sensitivity [4]. In the present paper, we estimate the errors of temperature measurements by pyrometers based on multielement RGB photodetectors (R — red, G — green, B — blue).

Conditions of Formation of Frames and Causes of the Appearance of Fluctuations of Pyrometric Signals. The functional diagram of the considered optical pyrometer and the design type of the photosensitive part of RGB matrices are presented in Fig. 1. The heat radiation of the object being controlled is focused by the lens on the surface of the photodetector matrix and, passing through the microlenses and the mosaic of Bayer light filters with G, B, G, B alternation on odd lines and R, G, R, G alternation on even lines, gets into the photosensitive cells. The absorption of photons in these cells leads to the generation of electric charges [5, 6], whose mean value can be calculated by integrating the photon flux over the spectrum and taking into account the spectral characteristics of the pyrometer:

$$Q_{k,\mathrm{ph}ji}(T) = tS_{ji}K_0\tau_{\mathrm{lens}}\int \tau_{\mathrm{f}}(\lambda)\,\varepsilon(x_i, y_j, \lambda, T)\,M^{\mathrm{bb}}(\lambda, T)\,\frac{\lambda}{hc}\,\eta_k(\lambda)\,d\lambda\,, \tag{1}$$

where $K_0 = [(l-f)^2/f^2]/(D^2 - 4l^2)$.

In controlling a uniformly heated body, the number of electrons accumulated in the matrix cells fluctuates about the mean values, the deviation from which is caused by the summed influence of the radiation, dark-current, and geometrical noises, as well by the noise of the output stage of charge reading.

Belarusian State University, 4 Nezavisimost' Ave., Minsk, 220030, Belarus. Translated from Inzhenerno-Fizicheskii Zhurnal, Vol. 81, No. 6, pp. 1046–1057, November–December, 2008. Original article submitted December 11, 2007.

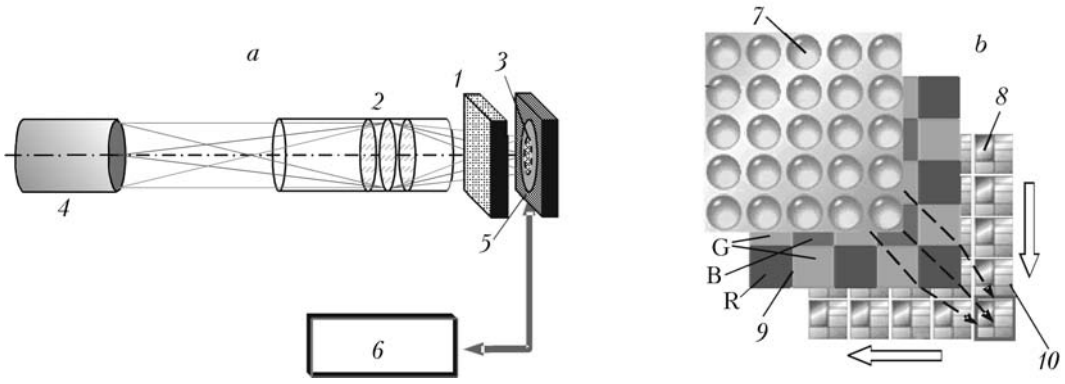

Fig. 1. Functional diagram of the recording part of the pyrometer (a) and of the design of the RGB matrix of photodetectors with a color mosaic of Bayer filters (b): 1) optical filter cutting off IR radiation; 2) lens with a hood; 3) object image; 4) object; 5) RGB matrix of photodetectors; 6) control unit of the matrix and pyrometric signal processing; 7) microlenses; 8) photosensitive elements; 9) mosaic of the Bayer filters; 10) transport registers.

The radiation noise is due to the fluctuations of the number of photons N_{ph} getting into a photodetector cell in the time of exposure. The quantity N_{ph} obeys the Poisson distribution, which permits writing $\sigma_{Q_{\text{ph}}} = e\sqrt{\overline{N}_{Q_{\text{ph}}}}$, where $\overline{N}_{Q_{\text{ph}}} = \eta\overline{N}_{\text{ph}}$. In this case, the signal-to-noise ratio for the incident flux is proportional to $\sqrt{\overline{N}_{Q_{\text{ph}}}}$. The dark noise resulting from the thermogeneration of electrons in the photosensitive cells also obeys the Poisson distribution and is described by analogous quantities — the mean quantity $e\overline{N}_{Q_{\text{d}}}$ and the rms deviation (RMSD) equal to $\sigma_{Q_{\text{d}}} = \sqrt{e\overline{N}_{Q_{\text{d}}}}$. Then the mean values of charges accumulated by the matrix elements can be found by summing (1) with the mean value of the dark charge formed:

$$Q_{k,\Sigma ji} = Q_{k,\text{ph}ji} + Q_{\text{d}ji} = tS_{ji}\int \overline{S}\,(\lambda)\,E_{ji}\,(\lambda, T)\,d\lambda + Q_{\text{d}ji}\,(t, T)\,, \tag{2}$$

where $\overline{S} = \eta(\lambda)\lambda e/(hc)$. The quantity $Q_{\text{d}ji}(t, T)$ of the dark charge generated in a matrix cells due to the thermal fluctuations depends linearly on the time of accumulation.

The photosensitive cells of the matrix have a spread of sensitivities, which causes the so-called geometrical noise or noise of the sensitivity nonuniformity of the matrix [7]. The technologies of the leading manufacturers of silicon-based RGB matrices provide normal distribution of geometrical noise with a mean equal to zero, small RMSD $\sigma_{Q_{\text{g}}} \approx 10^{-2}e\sqrt{\overline{N}_{Q_{\text{ph}}} + \overline{N}_{Q_{\text{d}}}}$, and a negligible number of failure and "hot" elements.

In reading the charge relief formed in the time of exposure of a frame, the accumulated charges transform into voltage and then are converted into digital form. The obtained signals measured by the number of readings of the analog-to-digital converter (ADC) are defined by the charge $Q_{k,\Sigma ji}$ and the charge-to-voltage transformation coefficient k_{QU}:

$$U_{k,ji}\,(T) = k_{QU}Q_{k,\Sigma ji}\,(T)\,. \tag{3}$$

In the process of transformation of charge packets into voltage, reading noise caused mainly by the reading cascade noise of the matrix arises. It has a normal distribution with a zero mean value and an RMSD $\sigma_{Q_{\text{r}}}$, which in terms of the RMSD of the value of the read charge equals (15–20)e for quality specimens of matrices on CCD devices.

Figure 2 shows the typical spectral characteristics of a color CCD matrix with account for the filter cutting off infrared (IR) radiation, and Fig. 3 gives the numerically calculated temperature dependences of the average number of photo- and thermogenerated electrons in photosensitive cells. For comparison, Fig. 3 presents also the dependences of RMSDs of the radiation, dark-current, and geometrical noises and the reading noise on the blackbody (bb) temperature. The focal length of the lens was assumed to be equal to 0.05 m, the distance to the bb model was 1 m, the relative aperture of the lens was $D/f = 1/2.8$, and the accumulation time was $t = 4\cdot10^{-2}$ sec. As is seen from Fig. 3, geometrical noise prevails, and the influence of the dark-current noises under the given measurement conditions is negligible.

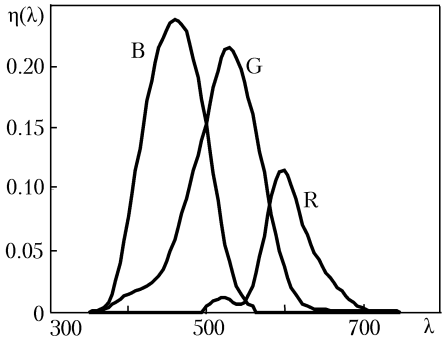

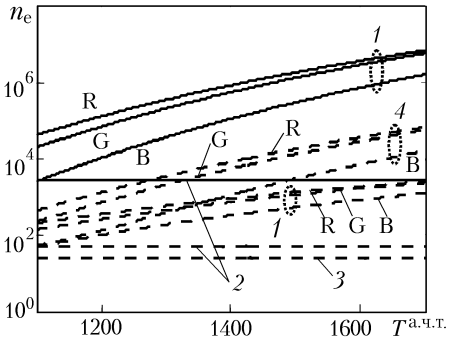

Fig. 2. Quantum efficiency of the ICX411 matrix with account for the Canon filter cutting off IR radiation. λ, nm.

Fig. 3. Temperature dependences of the average number of photogenerated electrons in R, G, and B matrix elements [1) solid lines], RMSD of the number of photogenerated electron [1) dashed lines], the average number and RMSD of thermogenerated electrons [2) solid and dashed lines], RMSD of the reading noise (3), and RMSD of the geometric noise (4). T^{bb}, °C.

The convective air flows around the object's surface and their related processes of oxidation of the heated surface by atmospheric oxygen can contribute to the spatial-temporal fluctuations of pyrometric signals.

Upon completion of the process of video frame formation a time-fixed charge relief is formed. All information that can be used to determine the thermodynamic temperature is contained in the spatial distribution of the values of read signals in three regions of the spectrum. In reading them, a three-layer RGB matrix of pyrometric signals with sizes $(N_j/2) \times (N_i/2)$ is formed. Since in the Bayer matrix the number of green optical filters is twice that of red or blue ones, upon the formation of a G layer the signals from the green cells are summed and divided into two.

Determination of the Object Temperature from the RGB Image. The multispectral methods of monochromatic pyrometry considered in [1, 2] permit excluding the influence of the object's emissivity on the obtained values of the thermodynamic temperature for several kinds of functional dependence ε(λ, T). For instance, at linear approximation of the natural logarithm ε(λ, T)

$$\ln \varepsilon (\lambda, T) = a_0 (T) + a (T) \lambda \tag{4}$$

the temperature of the object is determined analytically by the measured values of its luminosity at three wavelengths [1]. For photodetectors with wide spectral portions of sensitivity, it is impossible to obtain analogous analytical expressions for calculating T. Therefore, the dependences of the ratios of pyrometric signals U_B/U_G and U_G/U_R on the temperature, the emissivity, and the spectral characteristics of the filter and photodetectors were investigated by the numerical methods [4]. It has been established that at the emissivity of the object described by formula (4) the ratios of pyrometric signals of RGB photodetectors

$$\frac{U_B}{U_G} = \frac{\int \tau_f (\lambda) \exp (a\lambda) M^{bb} (\lambda, T) \frac{\lambda}{hc} \eta_B (\lambda) d\lambda}{\int \tau_f (\lambda) \exp (a\lambda) M^{bb} (\lambda, T) \frac{\lambda}{hc} \eta_G (\lambda) d\lambda}, \quad \frac{U_G}{U_R} = \frac{\int \tau_f (\lambda) \exp (a\lambda) M^{bb} (\lambda, T) \frac{\lambda}{hc} \eta_G (\lambda) d\lambda}{\int \tau_f (\lambda) \exp (a\lambda) M^{bb} (\lambda, T) \frac{\lambda}{hc} \eta_R (\lambda) d\lambda} \tag{5}$$

can be approximated by the expressions

$$\frac{U_B}{U_G} (a, T) \approx m_{BG} + n_{BG} T + r_{BG} a T, \quad \frac{U_G}{U_R} (a, T) \approx m_{GR} + n_{GR} T + r_{GR} a T. \tag{6}$$

The first two pairs of coefficients m_{BG}, m_{GR} and n_{BG}, n_{GR} approximating the temperature dependences of ratios of pyrometric signals U_B^{bb}/U_G^{bb} and U_G^{bb}/U_R^{bb} provided $a = 0$ are related to the spectral characteristics of the pyrometer and are found in the process of its calibration by the bb model [8]

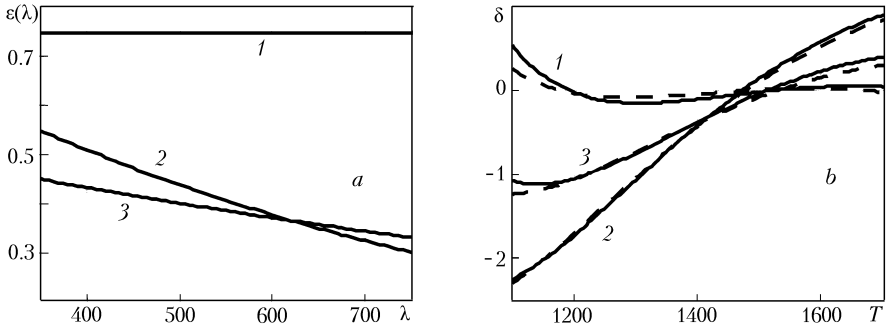

Fig. 4. Examples of exponential emissive powers (a) of iron and steel oxides at $a_0 \approx 0.75$, $a \approx 0$ (1), nonoxidized steel at $a_0 \approx 0.59$, $a \approx -0.78 \cdot 10^6$ m^{-1} (2), nonoxidized iron at $a_0 \approx 0.93$, $a \approx -1.52 \cdot 10^6$ m^{-1} (3), and their corresponding errors of approximations (b) of the pyrometric signal ratios U_B/U_G (solid curves) and U_G/U_B (dashed curves) by expression (6). λ, nm; T, °C; δ, %.

$$\begin{Bmatrix} m_{BG} \\ n_{BG} \end{Bmatrix} = \begin{Bmatrix} N_T & \sum_{n=1}^{N_T} T_n \\ \sum_{n=1}^{N_T} T_n & \sum_{n=1}^{N_T} T_n^2 \end{Bmatrix}^{-1} \begin{Bmatrix} \sum_{n=1}^{N_T} \frac{U_B^{bb}}{U_G^{bb}}(T_n) \\ \sum_{n=1}^{N_T} T_n \frac{U_B^{bb}}{U_G^{bb}}(T_n) \end{Bmatrix}, \quad \begin{Bmatrix} m_{GR} \\ n_{GR} \end{Bmatrix} = \begin{Bmatrix} N_T & \sum_{n=1}^{N_T} T_n \\ \sum_{n=1}^{N_T} T_n & \sum_{n=1}^{N_T} T_n^2 \end{Bmatrix}^{-1} \begin{Bmatrix} \sum_{n=1}^{N_T} \frac{U_G^{bb}}{U_R^{bb}}(T_n) \\ \sum_{n=1}^{N_T} T_n \frac{U_G^{bb}}{U_R^{bb}}(T_n) \end{Bmatrix}. \tag{7}$$

Errors in determining the above coefficients contributing to the systematic instrument temperature measurement error can be decreased by statistical averaging of measurements to the level of the bb model calibration error. The last pair of coefficients r_{BG} and r_{GR} approximating the temperature dependence of the pyrometric signal ratio on the value of a should be calculated by the formulas

$$r_{BG} = \frac{\sum_{n=1}^{N_T} \sum_{m=1}^{N_a} T_n a_m \left(\frac{U_B}{U_G}(a_m, T_n) - m_{BG} - n_{BG} T_n \right)}{\sum_{n=1}^{N_T} \sum_{m=1}^{N_{a1}} T_n^2 a_m^2}, \quad r_{GR} = \frac{\sum_{n=1}^{N_T} \sum_{m=1}^{N_{a1}} T_n a_m \left(\frac{U_G}{U_R}(a_m, T_n) - m_{GR} - n_{GR} T_n \right)}{\sum_{n=1}^{N_T} \sum_{m=1}^{N_{a1}} T_n^2 a_m^2}, \tag{8}$$

where the pyrometric signal ratios of U_B/U_G and U_G/U_R are calculated numerically with account for the spectral characteristics of the pyrometer which can be determined by means of a monochromator and the bb model [8].

Errors of approximation U_B/U_G and U_G/U_R by expressions (6) depend on the employed parameters of the functional dependence (4) and the width of the temperature range in which the pyrometer is calibrated. Figure 4 shows the typical spectral emissivities and the errors of approximation of the pyrometric signal ratios, that arise in using them, for a pyrometer with a spectral sensitivity complying with the conditions of Fig. 2. Breaking down the required temperature range of calibration into subranges, we can considerably decrease the approximation errors.

Approximations by (6) permit obtaining a simple analytical expression for determining the thermodynamic temperature of the metal surface

$$T = \xi_{BG} \frac{U_B}{U_G} + \xi_{GR} \frac{U_G}{U_R} + \xi_0, \tag{9}$$

where

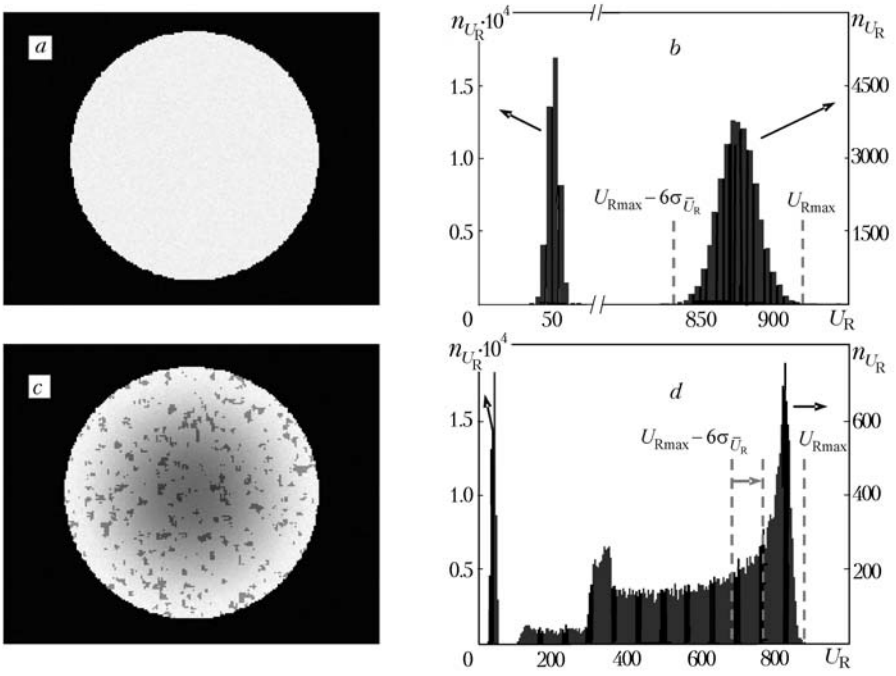

Fig. 5. R images of the face of a blank heated in an induction furnace at its uniform heating and in the absence of scale (a), at nonuniform heating and in the presence of scale (c), as well as pertinent histograms (b, d) obtained with the use of 10-digit quantization of pyrometric signals and with the RGB image size of 320 × 240. U_R, ADC reading.

$$\xi_{BG} = -\frac{r_{GR}}{n_{GR}r_{BG} - n_{BG}r_{GR}}; \quad \xi_{GR} = \frac{r_{BG}}{n_{GR}r_{BG} - n_{BG}r_{GR}}; \quad \xi_0 = \frac{-m_{GR}r_{BG} + m_{BG}r_{GR}}{n_{GR}r_{BG} - n_{BG}r_{GR}}.$$

Analogous expressions can also be obtained by approximating the emissivity by the power function $\varepsilon(\lambda, T) = b_0(T)(\lambda/\lambda_0)^{\beta(T)}$.

The formation of RGB photosensitive elements on one silicon crystal ensures long-time stability of the matrix parameters. But the small dimensions of the photosensitive elements and the small accumulation capacity of photogenerated charges lead to fluctuations of the arising charge relief caused by noises and the space-time inhomogeneity of radiation of the heated metal surface. To decrease errors in calculating T, it is necessary to average the pyrometric signals either over the object image area or over time, i.e., over the sequence of frames. Time-averaging under production conditions is inconvenient because in the main only dynamic thermal processes are controlled. Let us consider the specific features of the averaging of pyrometric signals over the object image area.

The surface of ferrous metals upon heating oxidizes nonuniformly, which leads to an inhomogeneity of the emissivity. Simultaneously with the oxide film growth a temperature inhomogeneity of the thin emitting layer of the surface develops. Therefore, in most production tasks for correct determination of the maximum temperature, one has to solve the problem of choosing the most luminous portions of the image, whose pyrometric signals are not distorted by the influence of the dielectric film of oxides. Highly oxidized portions of the surface as a result of the low heat conductivity of the thick oxide film are cooled faster by convective air flows, and their luminosity decreases. It is expedient to resolve nonoxidized luminous regions of the surface by the histogram of the R-layer of the image having a better signal-to-noise ratio. As is seen from Fig. 5b, with a uniformly heated body this histogram has a clearly defined two-mode character. The portion of the histogram with signal values from 800 to 950 ADC readings corresponds to the object, and that with about 50 readings of the ADC corresponds to the background. At a nonuniform temperature distribution and in the presence of strongly oxidized parts of the surface, whose temperature is much lower than the temperature of the weakly oxidized surface, the picture becomes more complicated — the portion of the histogram corresponding to the object stretches towards low luminosity values (Fig. 5c, d).

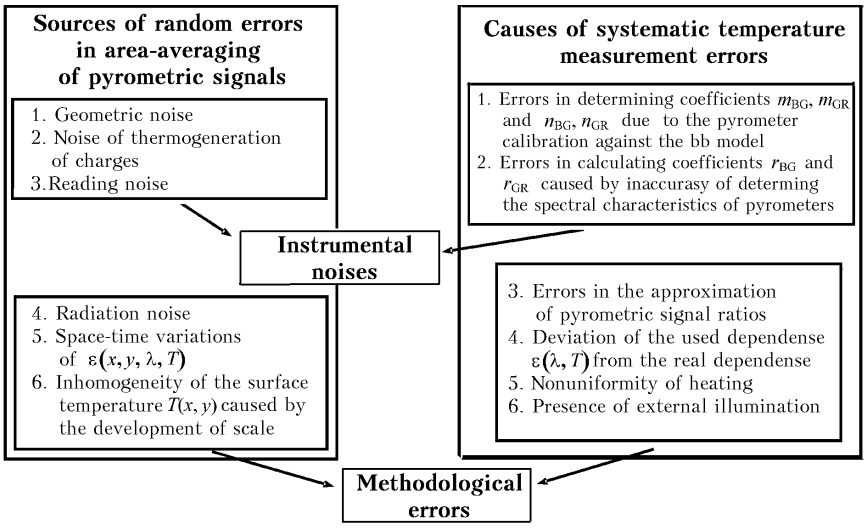

Fig. 6. Scheme of the formation of instrumental and methodological errors.

At a homogeneous temperature field of the object, averaging should be performed over the entire area of its image, i.e., by using, for obtaining $\overline{U}_R$, $\overline{U}_G$, and $\overline{U}_B$, only image pixels with addresses j and i, whose R-elements fall within the first mode of the histogram presented in Fig. 5b. To determine the maximum temperature at a nonuniform heating of the body, it is necessary to choose, for averaging, elements of its image with addresses defined by the position of R-layer cells with signal amplitude lying in the range $[U_{Rmax} - 6\sigma_{\overline{U}_R}, U_{Rmax}]$, where $\sigma_{\overline{U}_R}$ is the RMSD of R-signal fluctuations observed for a homogeneous temperature field. The dependence $\sigma_{\overline{U}_R}(\overline{U}_R) \approx \sigma_{\overline{U}_R}(U_{Rmax} - 3\sigma_{\overline{U}_R})$ is easily defined if the pyrometer is calculated against the bb model, since at values of accumulated charges exceeding $100e$ Poisson noises are described by the normal distribution.

Since in the matrix a small number of failure and "hot" elements are always present, it is better to choose the upper bound of the range of values of the signals in the R-layer U_{Rmax} participating in the averaging when at least a few tens of elements fall within the current interval of the hydrogram, and the object image should occupy the major part of the frame. Because the elements of parts of the objects image with a lower temperature also fall within the chosen range, the thus calculated temperature value, as calculations show, will be about 1% lower than the true value. This methodological error for particular kinds of inhomogeneity of the temperature field is eliminated by shifting the left bound of the range $[U_{Rmax} - 6\sigma_{\overline{U}_R}, U_{Rmax}]$ to the right.

To estimate the limits of applicability of the considered method of T determination, it is necessary to clarify the values of its inherent errors.

Temperature Measurement Errors. Measurement errors in pyrometry T are usually subdivided into instrumental errors that are largely due to the inaccuracy of determining pyrometric signals and methodological errors connected with the chosen methods of approximation of signals and T calculation, the difference of the used characteristics ($\varepsilon(x_i, y_j, \lambda, T)$ and $T(x_i, y_j)$) from the characteristics of the real object, and the presence of external illumination [1, 2], which is demonstrated by the scheme in Fig. 6.

In the pyrometers under consideration, the random component of the instrumental error is caused by recording track noises, and the systematic one by its calibration errors and inaccurate determination of its spectral characteristics. The contribution of radiation noises to the T measurement error is estimated similarly to the contribution of pyrometer noises. Therefore, we shall first estimate the contribution of random components to the total error.

The analytical expression for describing the dependence of the relative error in determining the temperature of the object on the relative measurement errors of pyrometric signals $\delta U_B/U_B$, $\delta U_G/U_G$, and $\delta U_R/U_R$ can be found by differentiating expression (9) with respect to variables U_B, U_G, and U_R:

$$\frac{\partial T}{\partial U_B} = \xi_{BG}\frac{1}{U_G}, \quad \frac{\partial T}{\partial U_G} = \xi_{BG}\frac{-U_B}{U_G^2} + \xi_{GR}\frac{1}{U_R}, \quad \frac{\partial T}{\partial U_R} = \xi_{GR}\frac{-U_G}{U_R^2}. \tag{10}$$

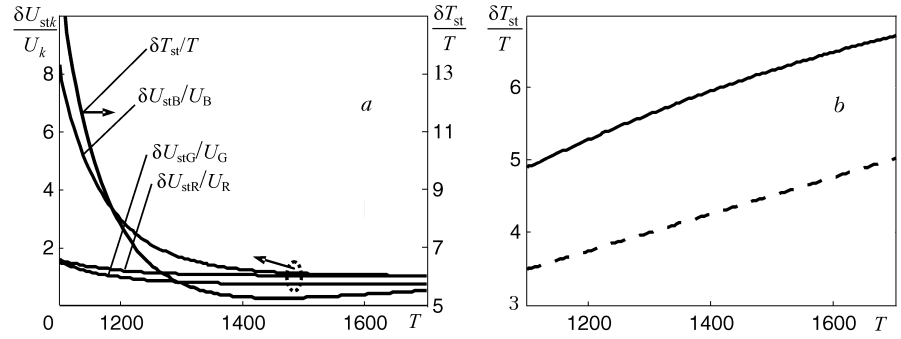

Fig. 7. Random errors in measurements of pyrometric signals and error, caused by them, in determining the temperature by its calculation by one pixel of the RGB image (a), as well as random errors in determining the temperature by the proposed method (solid curve) and by the three-wave monochromatic method of determinate pyrometry (dashed curve) at linear approximation of $\ln \varepsilon(\lambda)$ (b). T, °C; $\delta T_{st}/T$, $\delta U_{stk}/U_k$, %.

Having given for each spectral region the relative errors in the form

$$\frac{\partial T_B}{T} = \xi_{BG}\frac{1}{U_G}\frac{1}{T}\frac{U_B}{U_B}\partial U_B = \left(\xi_{BG}\frac{U_B}{U_G}\frac{1}{T}\right)\left(\frac{\partial U_B}{U_B}\right),$$

$$\frac{\partial T_G}{T} = \left(\xi_{BG}\frac{-U_B}{U_G^2} + \xi_{GR}\frac{1}{U_R}\right)\frac{1}{T}\frac{U_G}{U_G}\partial U_G = \left(\left(\xi_{BG}\frac{-U_B}{U_G} + \xi_{GR}\frac{U_G}{U_R}\right)\frac{1}{T}\right)\left(\frac{\partial U_G}{U_G}\right), \qquad (11)$$

$$\frac{\partial T_R}{T} = \xi_{GR}\frac{-U_G}{U_R^2}\frac{1}{T}\frac{U_R}{U_R}\partial U_R = \left(\xi_{GR}\frac{-U_G}{U_R}\frac{1}{T}\right)\left(\frac{\partial U_R}{U_R}\right),$$

we obtain the expression for the random component of the relative error

$$\frac{\delta T_{st}}{T} = \frac{1}{T}\sqrt{\left(\xi_{BG}\frac{U_B}{U_G}\right)^2\left(\frac{\delta U_{stB}}{U_B}\right)^2 + \left(\xi_{BG}\frac{-U_B}{U_G} + \xi_{GR}\frac{U_G}{U_R}\right)^2\left(\frac{\delta U_{stG}}{\sqrt{2U_G}}\right)^2 + \left(\xi_{GR}\frac{-U_G}{U_R}\right)^2\left(\frac{\delta U_{stR}}{U_R}\right)^2}, \qquad (12)$$

where $\delta U_{stk}/U_k \approx \delta U_{stk}/\overline{U}_k = \sqrt{\sigma^2_{U_{kf}} + \sigma^2_{U_{kd}} + \sigma^2_{U_{kr}} + \sigma^2_{U_{kg}}}/\overline{U}_k$.

Figure 7a shows the temperature dependences of the random errors $\delta U_{stk}/U_k$ in measuring pyrometric signals and of the random error $\delta T_{st}/T$, caused by them, in determining the temperature of the bb model. It is seen that the value of $\delta U_{stk}/U_k$ is maximum in the blue region of the spectrum, since the values of pyrometric signals in it are the lowest. With increasing temperature of the object the contribution of the radiation noise to random errors $\delta U_{stB}/U_B$, $\delta U_{stG}/U_G$, $\delta U_{stR}/U_R$ decreases, and the greatest contribution is made by the geometric noise of the matrix. Figure 7b gives the estimates of the total random error in the temperature measurement by the proposed method (solid curve) and by the three-wave method of determinate pyrometry (dashed curve) with monochromatic spectral channels [1], whose wavelengths λ_1, λ_2, λ_3 correspond to the maxima of the spectral quantum efficiency of the R, G, and B photosensitive elements of the matrix. In the calculations, it was assumed that the relative instrumental errors in measuring pyrometric signals are equal and are determined by geometric noises, i.e., $\delta U_{stB}/\overline{U}_B = \delta U_{stG}/\overline{U}_G = \delta U_{stR}/\overline{U}_R = 0.01$. It is seen that the relative error in determining the temperature by the proposed method in the 1100–1700°C range is about 1.5 times greater than the analogous error of the three-wave monochromatic method of determinate pyrometry. But averaging of the pyrometric signals over the area of the heated body image makes it possible to decrease the random error by a factor of $\sqrt{n_{el}}$. For example, at $n_{el} = 10^4$ $\delta T_{st}/T$ errors decrease by a factor 100.

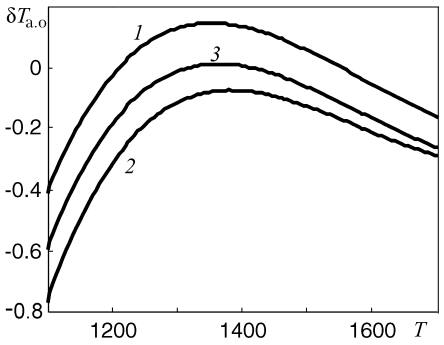

Fig. 8. Methodological temperature determination error caused by errors in approximations of pyrometric signal ratios by expressions (6) for the typical dependences ε(λ) (1, 2, and 3) presented in Fig. 4a. $\delta T_{a.r}$, %; T, °C.

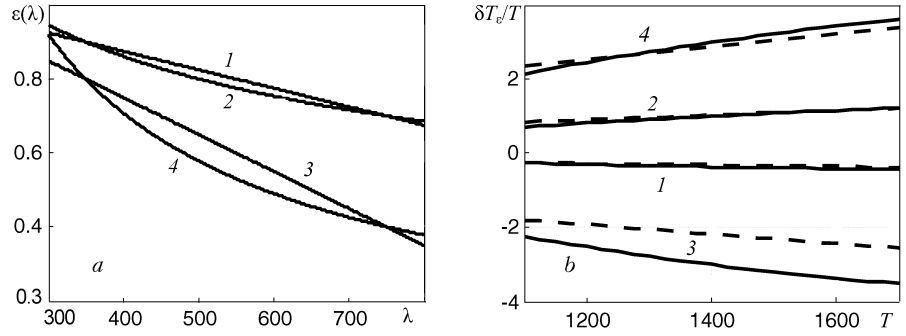

Fig. 9. Spectral emissive powers of the object described by the linear (1, 3) and power (2, 4) functions of the wavelength (a) and corresponding methodological errors in determining the temperature by the proposed method (solid curves) and by the three-wave monochromatic method of determinate pyrometry (dashed curves) (b). T, °C; $\delta T_\varepsilon/T$, %; λ, nm.

Systematic instrumental errors (Fig. 6) can be lowered to calibration errors of the bb model used. Therefore, systematic components of the methodological error prevail, and we will consider them in increasing order of their contribution.

The temperature measurement errors caused by the deviation of the real values of the ratios U_B/U_G and U_G/U_R from approximations (6) for the typical dependences ε(λ) (Fig. 4a) are given in Fig. 8. Note that if it is necessary to markedly decrease them, one should break down the range of measured temperatures into several subranges and calibrate the pyrometer against the bb model within their limits.

To estimate the systematic error caused by the difference of the real dependence ε(λ) from the exponential approximation used, we can use expression (12) substituting into it the corresponding changes in the pyrometric signals:

$$\frac{\delta U_{\varepsilon k}}{U_k} = \frac{\int \tau_f(\lambda)\,[\varepsilon(\lambda) - \exp(a_0 + a\lambda)]\,M^{bb}(\lambda, T)\,\frac{\lambda}{hc}\,\eta_k(\lambda)\,d\lambda}{\int \tau_f(\lambda)\exp(a_0 + a\lambda)\,M^{bb}(\lambda, T)\,\frac{\lambda}{hc}\,\eta_k(\lambda)\,d\lambda}.$$

Because of the complex dependence ε(λ, T) on the kind of metal and the state of its surface [9, 10], there are no agreed-upon approximations of the dependence of the emissivity of ferrous metals on λ and T. Usually, ε decreases with increasing λ, and oxidation of the surface upon heating leads to an approximation of ε to the emissivity of the oxide film weakly depending on the wavelength. Therefore, we shall demonstrate the behavior of the considered error for two kinds of possible deviations. Figure 9a shows the spectral emissive powers of the object given by the linear $\varepsilon(\lambda) = d_0 + d_1\lambda$ (curves 1 (d_0 = 1.075, $d_1 = -5.0\cdot10^5$ m^{-1}), 3 (d_0 = 1.15, $d_1 = -1.0\cdot10^6$ m^{-1})) and power ε(λ)

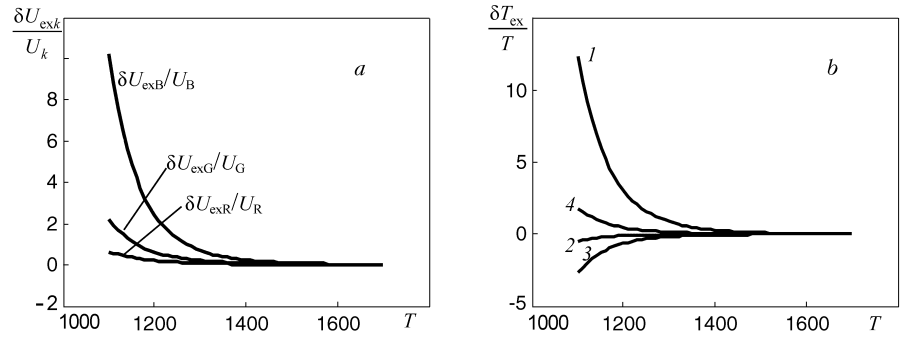

Fig. 10. Measurement errors of pyrometric signals (a) caused by external illumination equal to 50 lx and radiation with a color temperature of 4100 K, and errors in determining the object temperature $\delta T_{ex}/T$ (b) without compensation for the illumination (1), as well as with subtracting its contribution at known values of ε_B^{eff}, ε_G^{eff}, ε_R^{eff} (2) and at deviations of the real values of ε_B^{eff}, ε_G^{eff}, ε_R^{eff} from the used ones by 0.1 (3) and –0.1 (4). T, °C; $\delta U_{exk}/U_k$, $\delta T_{ex}/T$, %.

$= b_0(\lambda/\lambda_0)^{\beta}$ (curves 2 (b_0 = 0.9, β = –0.33, λ_0 = 350 nm) and 4 (b_0 = 0.8, β = –0.91, λ_0 = 350 nm)) functions of λ, and Figure 9b gives the corresponding temperature dependences $\delta T_\varepsilon/T$.

The approximation coefficients a_0 and a of these emissive powers by the exponential functions (4) were determined by the least square technique. It is seen that the considered error of the proposed method of T determination is practically at par with the three-wave monochromatic method of determinate pyrometry. It should be noted that to suppress this error, in the monochromatic method it is essential that $\varepsilon(\lambda)$ be described exactly by the exponential function (4) at the operating wavelengths λ_B, λ_G, λ_R. And the application of the proposed wide-spectrum method does not require such a coincidence. In this case, equality to zero of integrals $\int \tau_f(\lambda)(\varepsilon(\lambda) - \exp(a_0 + a\lambda))M^{bb}(\lambda, T)\frac{\lambda}{hc}\eta_k(\lambda)d\lambda$ in RGB spectral regions must be fulfilled.

For exact temperature measurement of the body in the region of maximum heating, we can form in it a hole whose radiation is close to the bb radiation [11].

The value of the error due to the external illumination depends on the spectral composition of the illumination $E_{ex}(\lambda)$ and the bihemispherical reflection coefficient of the body surface [1]. Since in production tasks it is common to measure the temperature of the lateral surfaces of heated bodies on which mainly scattered rays of employed optical sources are incident, to estimate this error, one can use expression (12), where U_k denotes pyrometric signals in the absence of external illumination, and their increments δU_{exk} in its absence are defined as follows:

$$\delta U_{exk} = tS_{ji}K_0\tau_{lens}\int \tau_f(\lambda)\,[1 - \varepsilon(\lambda)]\,E_{ex}(\lambda)\,\frac{\lambda}{hc}\,\eta_k(\lambda)\,d\lambda\,. \tag{13}$$

For illustration, Fig. 10a presents the measurement errors δU_{exk} of pyrometric signals from the surface with $\varepsilon(\lambda)$ shown in Fig. 4a (curve 3) at a level of its illumination equal to 50 lx by an external scattered luminous flux with a color temperature of 4100 K. It is seen that the temperature measurement error caused mainly by the external illumination in the blue region of the spectrum may exceed 10% (Fig. 10b, curve 1). Correction of measured pyrometric signals by subtracting from them δU_{exk} components that are due to the external illumination ($U_k = U_{exk} - \delta U_{exk}$) is possible with the use of a test area located near the object being controlled with known effective bihemispherical reflection coefficients ρ_{tk}^{eff}. In so doing, the contribution of the external illumination is determined by the measured signals of the test area image U_{tk} with account for ρ_{tk}^{eff} and ε_k^{eff}:

$$\delta U_{exk} \approx U_{tk}\left(1 - \varepsilon_k^{eff}\right)/\rho_{tk}^{eff} = U_{tk}\left(1 - \varepsilon_k^{eff}\right)/\left(1 - \varepsilon_{tk}^{eff}\right). \tag{14}$$

Such an approach permits decreasing by an order of magnitude errors caused by variations in the external illumination. Then the total systematic methodological errors in determining the temperature will be largely determined by the de-

viations of the real values of the object's emissive power from the exponential approximation. With exact correspondence of $\varepsilon(\lambda, T)$ to relation (4) the relative total systematic methodological errors of temperature determination can be lowered to 1%.

Conclusions. The estimation of errors in determining the thermodynamic temperature of metals by pyrometers based on multielement RGB photodetectors has shown that it is expedient to use them for monitoring technological processes in machine building connected with heat treatment. The proposed method of choosing the most luminous parts of the RGB image obtained makes it possible to considerably decrease the influence of the spatial inhomogeneity of optical properties of an emitting surface on the results of determining its maximal temperature. The simultaneous recording of pyrometric signals in the three spectral regions makes it possible, in using the proposed approximation of the pyrometric signal ratios, to calculate the current thermodynamic temperature of surfaces with an emissive power described by the exponential and power functions $\varepsilon(\lambda, T)$ even upon dynamic changes in the parameters of these functions in the heating process. The largest errors in determining the thermodynamic temperature are caused by the presence of external illumination, whose contribution to pyrometric signals should be taken into account. When its influence is eliminated, the value of the total errors will be largely determined by the deviation of the real dependence $\varepsilon(\lambda, T)$ from the used dependence.

NOTATION

a, a_0, b_0, β, λ_0, d_0, d_1, coefficients in the functions approximating the spectral emissive power; c, vacuum velocity of light; D, f, diameter and focal length of the lens, m; E_{ji}, illumination of the photosensitive matrix elements with numbers of lines and columns j and i, W/m^2; E_{ex}, illumination of the object by external background radiation, W/m^2; e, electron charge; h, Planck constant; i, j, numbers of matrix lines and columns; K_0, coefficient relating the luminosity of the object and the illumination of the matrix; k_{QU}, accumulated charge-to-voltage conversion factor, V/C; l, distance between the pyrometer and the object, m; M^{bb}, spectral luminosity of the blackbody, W/m^2; m_{BG}, m_{GR}, n_{BG}, n_{GR}, r_{BG}, r_{GR}, k_{BG}, k_{GR}, coefficients of approximating polynomials; N_j, N_i, numbers of lines and columns in the used matrix of photodetectors; N_{ph}, number of photons getting into a photodetector cell in the time of exposure; $\overline{N}_{Q_{ph}}$, $\overline{N}_{Q_d}$, average number of photogenerated and thermogenerated electrons formed in the photosensitive matrix cell in the time of exposure; N_T, N_a, numbers of temperature values of the blackbody model and the coefficient a, for which pyrometric signals are determined by pyrometer calibration; n_e, number of electrons; n_{el}, number of image elements (pixels) participating in the averaging over the object image area; n_{U_R}, number of pixels of the R-layer of the object image, for which the pyrometric signal value gets into a given column of the R-layer histogram; $Q_{k,phji}$, Q_{djji}, $Q_{k,\Sigma ji}$, photogenerated, thermogenerated, and total charges in a photosensitive matrix cell with line and column numbers j and i, C; S_{ji}, area of the photosensitive matrix cell of photodetectors, m^2; $\overline{S}$, mean conversion transconductance of matrix elements, C/(J·m); T, thermodynamic temperature, K; T^{bb}, temperature of the blackbody model, K; $T(x_i, y_j)$, temperature of the part of the surface whose image falls on a photosensitive cell with line and column numbers i and j, K; t, exposure of a frame, sec; x_i, y_j, coordinates of the part of the object surface whose image falls on a photosensitive cell with line and column numbers j and i; U_k, U_k^{bb}, voltages of the pyrometric signal from the object and from the blackbody model in the kth spectral channel at the exit from the ADC, V; $\overline{U}_k$, $U_{k\max}$, mean and maximum values of the pyrometric signal voltage in the kth spectral channel at the exit from the ADC, V; U_{tk}, voltage of the pyrometric signal from the test area in the kth spectral channel, V; U_{exk}, voltage of pyrometric signals from the object in the presence of background radiation, V; $\delta T_{a.r}/T$, temperature measurement error caused by approximation errors of pyrometric signal ratios; $\delta T_{ex}/T$, temperature measurement error caused by the influence of external illumination, %; $\delta T_{st}/T$, total random error of temperature measurement, %; $\delta T_\varepsilon/T$, temperature measurement error due to emissive deviations from the exponential approximation, %; δU_{exk}, pyrometric signal increment in the kth spectral channel as a result of the influence of external illumination, V; $\delta U_{stk}/U_k$, random measurement error of the pyrometric signal in the kth spectral channel, %; $\delta U_{\varepsilon k}/U_k$, pyrometric signal measurement error in the kth spectral channel due to emissive power deviations, %; ε, emissive power; $\varepsilon(x_i, y_j, \lambda, T)$, emissive power of the part of the surface whose image falls on a photosensitive cells with line and column numbers i and j; ε_k^{eff}, ε_{tk}^{eff}, effective emissive power of the object and the test area for the kth spectral channel; η, quantum efficiency, m^{-1}; η_k, quantum efficiency of matrix elements in the kth spectral range, m^{-1}; λ, radiation wavelength, m; λ_B, λ_G, λ_R, wavelengths corresponding

to the maximum quantum efficiency of photodetector jointly with the optical filter in the R, G, and B spectral channels, nm; ρ_{tk}^{eff}, effective reflection coefficient of the test area; τ_{lens}, transmission of the pyrometer lens; $\tau_f(\lambda)$, spectral transmission of the optical filter; $\sigma_{Q_{\text{ph}}}$, σ_{Q_d}, σ_{Q_r}, σ_{Q_g}, RMSD of the photogenerated charge, the thermogenerated charge, the reading noise, and the geometric noise, C; $\sigma_{U_{k\text{ph}}}$, $\sigma_{U_{kd}}$, $\sigma_{U_{kr}}$, $\sigma_{U_{kg}}$, RMSD of the radiation, dark current, geometric, and reading noises in the *k*th spectral channel at the exit from the ADC, V. Subscripts: d, dark current; eff, effective; ex, external; g, geometric; ph, photon; r, reading; st, stochastic; t, test; a.r, approximation of the ratio; bb, blackbody; lens, lens; f, filter; el, element; max, maximum.

REFERENCES

1. V. N. Snopko, *Methods of Pyrometry Using the Thermal Radiation Spectrum*, B. I. Stepanov Inst. of Physics, Minsk (1999).
2. D. Ya. Svet, *Optical Methods of Measurement of Actual Temperatures* [in Russian], Nauka, Moscow (1982).
3. K. Chrzanowski and M. Szulim, Error of temperature measurement with multiband infrared systems, *Appl. Opt.,* **38**, No. 10, 1998–2006 (1999).
4. A. G. Sen'kov and V. A. Firago, Three-spectrum pyrometry of metals based on modern three-color multielement photodetectors, *Vestn. BGU*, *Ser.* 1, No. 1, 54–61 (2007).
5. V. A. Firago, *Radiation Detectors*, *Synopsis of Lectures* [in Russian], BGU, Minsk (2005).
6. V. A. Firago, Determination of the optimum radius of the Gaussian function of lens scattering in detecting point objects by systems with image discretization, *Vestn. BGU*, *Ser.* 1, No. 1, 28–33 (2006).
7. S. M. Sze, *Physics of Semiconductor Devices* [Russian translation], in 2 volumes, Mir, Moscow (1984).
8. V. A. Firago, A. G. Sen'kov, and V. Vuitsik, Calibration of spectral ratio pyrometers with VGA matrices of photodetectors, in: *NEET 2007: Proc. 5th Int. Conf.*, 12–15 June, Zakopane, Poland (2007), p. 102.
9. N. A. Rubtsov, E. I. Averkov, and A. A. Emel'yanov, *Thermal Radiation Properties of Materials in the Condensed State* [in Russian], Inst. Teplofiz. SO AN SSSR, Novosibirsk (1988).
10. S. G. Agababov, On the effect of secondary roughness on the radiative properties of solids, *Teplofiz. Vys. Temp.*, **8**, No. 1, 220–222 (1970).
11. A. G. Sen'kov and V. A. Firago, Reduction of methodological errors in determining the temperature of metals by two-color pyrometers, *Inzh.-Fiz. Zh.*, **79**, No. 4, 135–138 (2006).